metals

MDPI

Article

Fatigue Response of As-Built DMLS Maraging Steel and Effects of Aging, Machining, and Peening Treatments

Dario Croccolo [1], Massimiliano De Agostinis [1], Stefano Fini [1], Giorgio Olmi [1,*], Francesco Robusto [1], Snežana Ćirić Kostić [2], Aleksandar Vranić [2] and Nebojša Bogojević [2]

[1] Department of Industrial Engineering (DIN), University of Bologna, 40136 Bologna, Italy; dario.croccolo@unibo.it (D.C.); m.deagostinis@unibo.it (M.D.A.); stefano.fini@unibo.it (S.F.); francesco.robusto2@unibo.it (F.R.)

[2] Faculty of Mechanical and Civil Engineering in Kraljevo, University of Kragujevac, Kraljevo 36000, Serbia; cirickostic.s@mfkv.kg.ac.rs (S.Ć.K.); vranic.a@mfkv.kg.ac.rs (A.V.); bogojevic.n@mfkv.kg.ac.rs (N.B.)

* Correspondence: giorgio.olmi@unibo.it; Tel.: +39-051-2093455 or +39-0543-374427

Received: 9 June 2018; Accepted: 25 June 2018; Published: 29 June 2018

Abstract: The main motivations for this study arise from the need for an assessment of the fatigue performance of DMLS-produced Maraging Steel MS1, when it is used in the "as fabricated" state. The literature indicates a lack of knowledge from this point of view; moreover, the great potentials of the additive process may be more and more incremented, if an easier and cheaper procedure could be used after the building stage. The topic has been tackled experimentally, investigating the impact of heat treatment, machining, and micro-shot-peening on the fatigue strength with respect to the "as built state". The results indicate that heat treatment may improve the fatigue response, as an effect of the relaxation of the process-induced tensile residual stresses. Machining can also be effective, but it must be followed (not preceded) by shot-peening, to benefit from the compressive residual stress state generated by the latter. Moreover, heat treatment and machining are related by a strong positive interaction, meaning their effects are synergistically magnified when they are applied together. The experimental study has been completed by fractographic as well as micrographic analyses, investigating the impact of the heat treatment on the actual microstructure induced by the stacking process.

Keywords: Additive Manufacturing (AM); Direct Metal Laser Sintering (DMLS); Maraging Steel; "as built" state; heat treatment; machining; shot-peening

1. Introduction

The Additive Manufacturing (AM) process is based on layer manufacturing without any additional tools or machining processes. Direct Metal Laser Sintering (DMLS) and Selective Laser Melting (SLM) are two promising Additive Manufacturing technologies. Both of them are powder bed-based technologies [1–6].

The concept of layered built parts dates from more than one century ago. AM enables manufacturing without tools, using just one AM machine fed by a CAD model. This is split into two-dimensional layers with constant thickness, by specific software; the layers can be regarded as areas that will be melted with proper thickness. Every new layer is fused with the previous one during the AM process. The part is progressively built, repeating this process until the last layer is stacked.

There are several AM technologies, depending on the handled material, on how the material is applied or fused, etc. Powder Bed technology is based on material application on the entire building

surface; afterwards, the laser or electron beam melts the area that corresponds to the sliced surface. The process is repeated until part completion. Wire or powder feed technology is based on the step-by-step material application and melting until the surface that corresponds to the sliced layer is formed. In this case, the material is applied to the surface that is being manufactured only. A further classification of the AM techniques deals with the principle of material melting (laser beam, electro beam, electro-arc etc.). In almost all the technologies for AM of metal parts, the material is completely melted and bonding between layers is achieved during solidification. DMLS and SLM are nowadays quite close technologies [5,6]. A slight difference between them arises from the mechanism of powder fusion. In particular, in the case of SLM, a full melting occurs, whereas for DMLS, selective laser sintering causes the powder to fuse together. Anyway, they are commonly regarded as basically the same technique, being grouped under the powder bed fusion technologies according to the Standard [7]. The aforementioned different acronyms mostly arise from different trademarks, which both aim at stressing the use of laser as power source.

At the early stages of development of these technologies, components after manufacturing were remarkably porous, as not full density could be achieved, due to partial fusion. The melting and sintering processes were different, and the processed materials were mainly based on Iron, Copper and Nickel alloy. Moreover, additional processing was mandatory, to achieve better density and fusion [8,9].

AM technologies are more and more used in the industrial field and are also attracting interest with regard to biomechanics. Using 3D CT scanners, it is possible to model custom implants that perfectly fit the person's need [10–12]. Materials with good bio-compatibility can be processed by AM, which gives them good potentials for dental and medical purposes [13].

The layer-based manufacturing provides a particular microstructure affecting the build parts that is different from the casted structure of the same wrought material. In AM, material melting and cooling rates are very high. Fast melting is the result of high energy concentration, whereas fast cooling arises from the small amount of melted material with low surrounding temperature. This high temperature gradient usually induces high tensile residual stresses. Part building starts on thick steel plate (base-plate). The part can be built directly on the plate or with an additional support structure, stacked between the plate and the part. Its purpose is part constraining; moreover, it facilitates heat flow from the part during the scanning (melting) process. The support structure needs to be strong enough to efficiently restrain any kind of deformation that residual stress can cause. The generation of a residual stress state affecting the fabricated component is indeed a drawback of this process that is usually tackled by suitable heat or surface treatments. Machine manufacturers usually provide some data regarding the mechanical properties of AM built parts in the material datasheets [14]. However, these mainly deal with static properties, such as ultimate tensile strength, yield strength, hardness, mechanical characteristics before and after ageing, etc. Therefore, there is a great interest towards the fatigue response and the impact of the post-manufacture treatments.

Maraging steel is one of the most promising materials, for use in Additive Manufacturing [15]. Density of AM built parts are generally higher than 90%. The hardness of AM-built parts from Maraging Steel is incremented up to 50 HRC after the aging heat treatment, thus making it well comparable to that of wrought material [14]. It has good mechanical properties, and it can be a good candidate for high-carbon steel substitution. It is resistant to corrosion and crack initiation during tempering and has good machinability [16–18]. It has a relatively high ultimate tensile strength (UTS) after the heat treatment, around 2000 MPa. Therefore, it is a promising material to be used for structures operating under high states of load in many fields. The mentioned properties become more attractive, considering that AM technologies gives the chance to build a multi-part object as a single part [19], making it possible to build monolithic complexly shaped components in small batches. Research contributions on the Fatigue limit (FL) and the fatigue strength (FS) of Maraging steel made by some of AM processes are quite limited, to the best of the authors' knowledge. A recent study is presented in [20]; however, this study is more devoted to the additively processed material performance under

low-cycle, rather than to its high cycle fatigue response, depending on different build or post-process parameters. The present paper presents a follow-up of a previous research by the same authors [21].

Components produced by AM can have different orientation with respect to the stacking direction of the layers. The aim of the previous research was to explore the effect of build orientation on the fatigue strength of Maraging Steel samples built by DMLS EOS M280 machine. The obtained results indicate that part orientation did not have significant effect on FS and FL when the parts were treated by micro-shot peening and heat treatment after the stacking process, thus meeting the powder producer recommendations. The components had then been machined with 0.5 mm allowance in order to get an optimal surface finishing. The aforementioned outcomes were also confirmed by the study [22] involving the same material. A further research [23] was then focused on Stainless Steel PH1 and led to a partial confirmation: some effect was observed in this case, probably due to different material properties and stacking parameters.

Literature studies dealing with the effects of the stacking process on the mechanical properties of the parts made by AM are few. Most research deals with the effects of the process parameters as well as of post-processing on tensile static strength [24–26]. Few papers are concerned with the fatigue strength of Aluminium alloy [27–29], Inconel alloy [30], and Titanium alloy [31]. Review papers have been written, trying to collect all the technologies and all the available mechanical testing results [32]. However, a lack of consistency between the testing procedures and the obtained results can be noticed, when all these data are merged together.

There is nowadays an increasing interest in lowering down post-manufacturing expenses in AM, and in speeding up the process from design to installation. Sometimes, post-processing is not possible, for instance, when treating lattice structures, cooling channels in injection moulds or in turbine blades. In particular, machining or shot-peening cannot be performed on internal surfaces; on the other hand, running a heat treatment could be expensive and time-consuming. This interest is also explored by some recent studies [6,33–35] that have dealt with the fatigue properties of Ti-6Al-4V or Stainless Steels in their as-built states, or with the effects of post-manufacture treatments. An intensive study is needed to clarify if post-processing treatments, including machining or heat treatment, can be skipped and, if so, how the best compromise between costs and strength can be accomplished. This was the main motivation that led to this study, whose aim was to investigate the effects of heat treatment, machining, and shot-peening on the fatigue response of DMLS-built Maraging Steel vs. the as-fabricated state.

Issues of novelty arise from the lack of extensive campaigns involving this material in the scientific literature, dealing with its response in the as-built state and with the joint effects and, possibly, the interaction of the aforementioned post-manufacture part-processing strategies. A further issue of novelty arises from the use of an ANOVA-based statistical method. This makes it possible to compare the determined S-N curves in the finite life domain and to assess the significance of the aforementioned effects and interactions.

This topic has been tackled experimentally: for this purpose, an experimental campaign has been arranged as a factorial plane, with a total amount of five treatment combinations. Fatigue tests have been run on all the sample types, finally working out the fatigue curves in the finite life domain and the fatigue limits. These results have then been compared and discussed, based on statistical methods.

2. Materials and Methods

The testing procedure was based on ISO 1143 Standard for rotating bending fatigue testing [36]. The Standard defines the testing procedure, the load scheme, and the specimen geometry. Specimens were designed with cylindrical smooth geometry with uniform 6 mm diameter at the gage. The smallest recommended dimension by the Standard has been chosen as the best compromise between Standard consistency and manufacturing costs. A sample drawing including its dimensions as well as dimensional and geometrical tolerances is shown in Figure 1. It must be pointed out that the specification regarding surface quality was not considered for the "as built" condition, to properly account for the effect of machining.

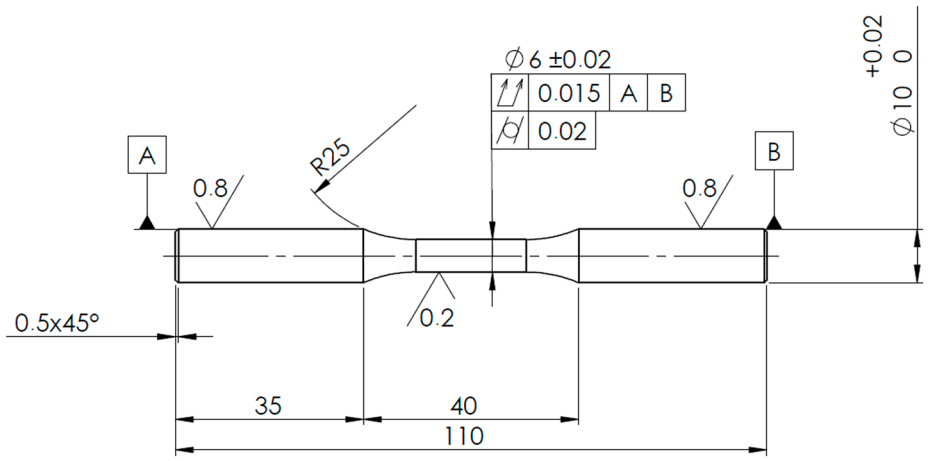

Figure 1. Smooth sample for fatigue tests under rotating bending according to [36] (all dimensions in mm, roughness in μm).

The specimens have been manufactured by M280 DMLS machine (EOS GmbH—Electro Optical Systems, Krailling, Germany), equipped by Ytterbium fibre laser with 200 W power and emitting 0.2032 mm thickness and 1064 nm wavelength infrared light beam [37]. Specimen material was MS1 Maraging steel MS1 (by EOS GmbH–Electro Optical Systems, Germany), equivalent to 1.2709 steel [38] and also reported as 18% Ni Maraging 300 or AISI 18Ni300. The chemical composition of the material is provided in Table 1. Specimen manufacturing was done in the processing chamber of the machine with working area of 250 × 250 mm in horizontal plane and with maximum building height up to 325 mm. The base plate was preheated to the temperature of 40 °C.

Table 1. Chemical composition of Maraging steel MS1.

Ni (%)	Co (%)	Mo (%)	Ti (%)	Al (%)	Cr (%)	Cu (%)	C (%)	Mn (%)	Si (%)	P (%)	S (%)	Fe (%)
17–19	8.5–9.5	4.5–5.2	0.6–0.8	0.05–0.15	≤0.5	≤0.5	≤0.03	≤0.1	≤0.1	≤0.01	≤0.01	Bal.

The Manufacturing process typically takes place in nitrogen inert atmosphere, generated from compressed air by nitrogen generator that is built inside the machine. The process chamber consists of three platforms and recoater: The Dispenser platform, where material powder is contained, the Building platform, on which the base plate is set and the building process is done, and the Collector platform for the collection of the excess material. A scheme of the building chamber is shown in Figure 2.

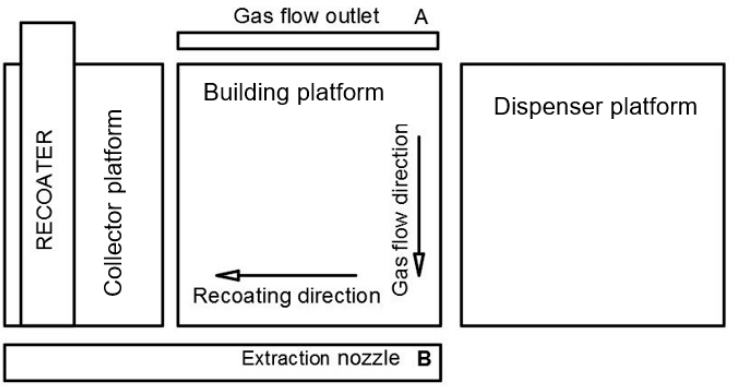

Figure 2. A scheme of the chamber of the utilized EOS machine.

The material was applied with 40 μm thickness that corresponds to the recommended layer thickness for MS1 Maraging Steel. The building parameters (laser speed, laser power, laser offset, layer thickness, etc.) of the EOSINT M280 for MS1 sample manufacturing were kept constant for all the stacking tasks. They were provided by the EOS as a predetermined set of parameters named "PERFORMANCE". This parameter set can be regarded as a good compromise between surface quality and manufacturing speed.

The scanning strategy consisted of parallel traces on every layer; layer by layer, the scanning strategy was rotated by an angle of 67°. The contour of the scanned surface was finally rescanned in order to get better surface quality. An example of the scanning process is shown in Figure 3a.

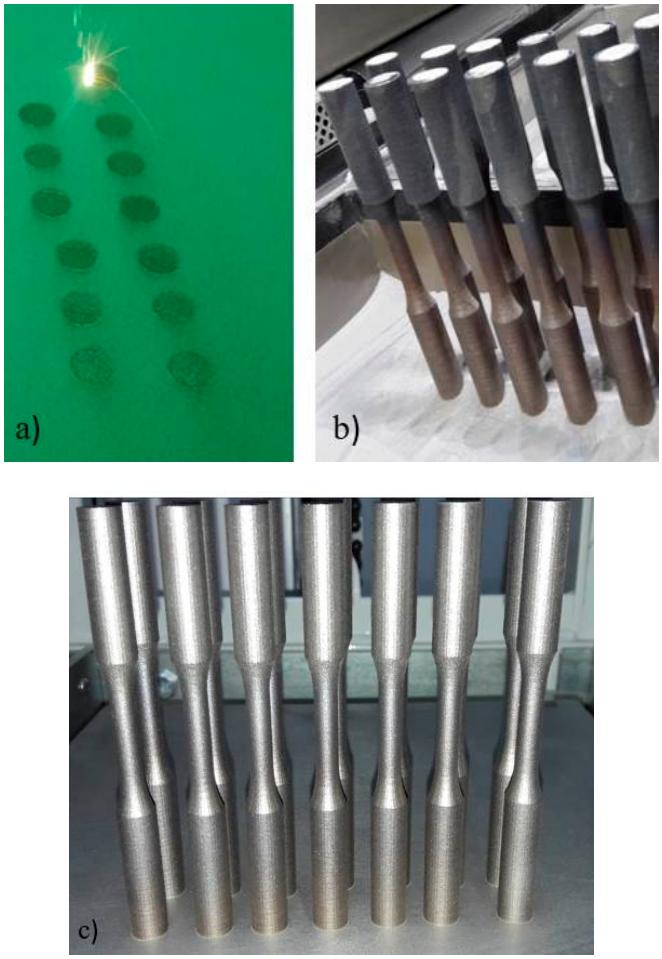

Figure 3. (**a**) As Built specimens during scanning; (**b**) Specimens cleaning from powder; (**c**) Specimens after micro-shot-peening.

The specimens were built directly on the base plate, with vertical orientation, without using a support structure (Figure 3c). Proceeding this way, the surface quality of the specimens in the as-fabricated state was unaffected by the support structure teeth traces on the surface, as conversely would have been with different build orientations. After the building process, the specimens were taken from the process chamber, cleaned from excessive powder by micro-shot-peening, using stainless steel spherical shots with 400 μm diameter under a flow pressure of 5 bar. This treatment is usually performed to close the process-induced porosities and to generate compressive residual stresses that reduce the tensile residual state induced upon fabrication. The samples were then cut off from the base plate, by wire cutting with Electrical Discharge Machining (EDM).

The samples planned for heat treatment underwent age-hardening by heating in oven. The temperature was increased from room temperature to 490 °C in 1 h; afterwards, they were kept at constant temperature for an additional 5 h (total 6 h process), before gradual cooling in fresh air. This heat treatment is usually recommended to achieve a reduction of the process-induced tensile residual stresses, with a potential beneficial effect on the fatigue response of the built parts [39,40]. Then, the specimens planned for machining, were ground with 0.5 mm allowance with the aim of achieving the surface quality requirement in the drawing in Figure 1, according to the ISO 1143 Standard [36], as well as to improve the fatigue performance.

The experimental campaign was arranged, according to the scheme in Table 2: in particular, the 2-by-2 design was run first, in order to investigate the impacts of heat treatment and machining with surface refinement. The sample set named N involved samples that underwent micro-shot-peening, but neither heat treatment nor machining. The samples from set M were micro-shot-peened and then machined, whereas those of set H underwent micro-shot-peening and subsequent aging treatment. Finally, for the HM condition, consisting in peened, heat-treated and machined samples, the curve determined in [22], integrating the results in [21], was used. As explained in this reference, this can be regarded as the most general and reliable model for the fatigue behaviour of Maraging Steel MS1 in the full treatment condition at the current state of the art.

Table 2. Design of the experimental campaign.

		Machining		
		No	**Yes**	**Yes, with Subsequent Shot-Peening**
Aging Heat Treatment	**No**	Set N	Set M	Set MP
	Yes	Set H	Set HM	

The experimental design was then completed by the addition of a further combination, named MP: in this case, the samples underwent machining just after fabrication and then shot-peening by steel shots with 0.7 mm diameter. This surface treatment was carried out with shot flow under 5 bar pressure. This latest combination was added to investigate the effect of the different post-processing order on the fatigue response. The main motivation supporting this choice was that, despite the material manufacturer recommendations, the beneficial residual stress state yielded by post-fabrication peening was likely to be completely removed by the subsequent machining with 0.5 allowance.

All the samples have undergone geometry measurement, to check that requirements have been met. Diameter dimension and surface roughness have been measured at the head and at the gage. For this purpose, a micrometre screw gage (with the resolution of 0.01 mm) and a portable surface roughness tester (with the resolution of 0.01 µm, Handysurf E-30A; Carl Zeiss AG, Oberkochen, Germany) have been used.

Diameter measurement checks have been done at two points at the heads, replicating measurement with 90° rotations at each point, for a total of eight replications, including both the specimen heads. Diameter at the gage was measured at three points, with two replications for each, by 90° rotation, for an overall number of 6 replications.

Surface roughness on both the heads and on the gage was measured over 8 replications. In particular, roughness was averaged over 4-mm runs along the longitudinal axis, considering 90° angled spots with two repetitions for each. Measurement at the gage was performed only on the samples that got broken during the fatigue testing, due to the impossibility of correctly aligning the roughness tester in the unbroken ones. However, the retrieved measurements were sufficient to get evidence of the roughness mean value at gage.

Some average values of the diameter and surface roughness measurements are provided in Table 3 with reference to Set N. For the sake of synthesis, the other results concerning the measured roughness are not provided. It is worth mentioning that, considering a mean value over all the manufactured samples, R_a at gage for the machined specimens (sets M, HM) is 0.5 µm. This value is remarkably

incremented, by almost one order of magnitude, up to 4.2 μm, for the samples that did not undergo machining (N, H). Finally, the peening treatment after machining also leads to a roughness increase up to 1 μm, as an effect of the dimples generated by shot impacts.

Table 3. Dimensional and roughness (R_a) measurements with regard to the samples of Set N.

Specimen ID	Gage Diameter			Head Diameter (Left Side)			Head Diameter (Right Side)		
	Mean (mm)	St. dev. (mm)	Roughness Ra (μm)	Mean (mm)	St. dev. (mm)	Roughness Ra (μm)	Mean (mm)	St. dev. (mm)	Roughness Ra (μm)
N.1	6.09	0.012	4.24	10.07	0.020	5.54	10.06	0.024	3.92
N.2	6.09	0.010	4.12	10.08	0.004	5.48	10.07	0.004	4.47
N.3	6.08	0.008	3.97	10.06	0.010	5.19	10.05	0.014	4.49
N.4	6.09	0.008	4.37	10.07	0.013	4.74	10.05	0.017	4.53
N.5	6.09	0.005	4.57	10.07	0.019	5.28	10.05	0.015	5.49
N.6	6.09	0.009	—	10.07	0.012	4.75	10.06	0.014	4.68
N.7	6.09	0.010	—	10.08	0.007	4.43	10.06	0.009	4.77
N.8	6.09	0.007	—	10.07	0.008	4.24	10.05	0.018	4.76
N.9	6.09	0.007	4.07	10.06	0.010	4.76	10.05	0.019	4.18
N.10	6.09	0.009	5.12	10.08	0.011	5.65	10.05	0.019	6.02
N.11	6.10	0.012	4.54	10.08	0.014	4.72	10.06	0.018	4.83
N.12	6.08	0.012	2.30	10.07	0.015	4.86	10.05	0.006	4.34
N.13	6.08	0.009	3.75	10.08	0.008	5.10	10.06	0.012	4.57
N.14	6.09	0.014	4.21	10.05	0.003	4.48	10.05	0.018	4.07

The fatigue tests were carried out, loading the samples under four-point rotary bending, using the same testing machine as in [21]. Tightening was done in such a way that specimen heads could not have any chance to revolve inside chuck collets. After the specimen was mounted, the radial misalignment of the gage section was checked, as recommended by the aforementioned Standard. Testing was performed with stress ratio R = −1 and with the frequency of 60 Hz. Each test was conducted in the load-controlled mode, applying a proper stress amplitude; related values are provided in full details in the next Section.

The samples were tested until failure or until 10^7 cycles to be regarded as run-out. Each sample set consisted of 7 to 15 specimens. Using the aforementioned procedure, it was possible to obtain FL and the S-N curve for finite life domain. The fatigue limit was obtained by the Dixon stair-case method for a small number of sample trials with failure or non-failure outcomes [41]. The Dixon method is a modified stair-case method that makes it possible to estimate FL even from small series of nominal trials (in this case, four to seven). Standard deviation was estimated to assess the uncertainty and to determine the confidence band for FL. ISO 12107 was used for processing the data in finite life domain [42]. Data were linearly interpolated in logarithmic diagrams. Upper and lower bounds of the logarithmic curve were determined, based on the standard deviation of fatigue life, with the probability of failure of 90% for upper limit and 10% for lower limit and with the confidence level of 90%.

Fractographic and micrographic analysis have been done as well for some samples, after the end of the testing campaign to examine fracture initiation and propagation areas. In particular, some specimens were cut, embedded into phenolic resin, and polished for micrographic analysis, as in Figure 4. The specimen surface was etched with combination of 150 cc of water (H_2O), 50 cc of Chloridric Acid (HCl), 25 cc of Nitric Acid (HNO_3), and 1 g of Calcium Chloride. Etching was done at room temperature for 70 s. A Stemi 305 stereo-microscope (by ZEISS, Oberkochen, Germany) has been utilized for fractographies, whereas an Optiphot-100 optical microscope (by Nikon, Melville, NY, USA) has been used for both micrographic and (more zoomed) fractographic analyses.

Figure 4. Sample preparation for micrographies, in particular the resin-embedded sample, (longitudinal and cross sections) is depicted on the right.

3. Results

The results of the testing campaign are collected in Tables 4–7. The Tables provide data regarding specimen ID, nominal stress amplitude at the gage, observed life (to be intended as the number of cycles to failure, N), and comment regarding the trial outcome. In particular, "Run-out" indicates that the specimen survived testing at given load after 10^7 cycles, whereas "Y" indicates that failure occurred. In this case, the number of cycles to failure is also reported.

Table 4. Results of the fatigue tests on the samples of Set N.

Specimen ID	Stress Amplitude (MPa)	Life (Cycles to Failure)	Failure
N.1	610	175,804	Y
N.2	550	236,637	Y
N.3	490	3,577,212	Y
N.4	430	8,336,653	Y
N.5	400	9,659,056	Y
N.6	370	—	Run-out
N.7	400	—	Run-out
N.8	430	—	Run-out
N.9	460	8,069,582	Y
N.10	430	—	Run-out
N.11	460	9,900,777	Y
N.12	610	151,212	Y
N.13	550	156,691	Y
N.14	490	687,908	Y

Table 5. Results of the fatigue tests on the samples of Set H.

Specimen ID	Stress Amplitude (MPa)	Life (Cycles to Failure)	Failure
H.2	579	65,841	Y
H.4	550	73,082	Y
H.7	520	169,324	Y
H.15	490	779,587	Y
H.1	460	—	Run-out
H.3	490	8,503,786	Y
H.5	460	198,385	Y
H.6	460	2,589,275	Y
H.16	430	—	Run-out
H.8	460	2,614,325	Y
H.9	579	100,886	Y
H.10	550	2,245,442	Y
H.17	490	—	Run-out
H.11	520	124,220	Y
H.12	490	131,030	Y
H.13	490	—	Run-out
H.14	550	640,238	Y

Table 6. Results of the fatigue tests on the samples of Set M.

Specimen ID	Stress Amplitude (MPa)	Life (Cycles to Failure)	Failure
M.1	610	81,160	Y
M.2	520	219,333	Y
M.3	460	2,415,186	Y
M.4	400	7,885,879	Y
M.5	370	3,035,027	Y
M.6	340	—	Run-out
M.7	370	7,879,073	Y
M.8	340	—	Run-out
M.9	370	—	Run-out
M.10	400	5,662,050	Y

Table 7. Results of the fatigue tests on the samples of Set MP.

Specimen ID	Stress Amplitude (MPa)	Life (Cycles to Failure)	Failure
MP.12	400	—	Run-out
MP.1	430	7,156,630	Y
MP.3	460	7,486,110	Y
MP.7	490	3,327,981	Y
MP.8	520	1,513,780	Y
MP.2	580	1,424,868	Y
MP.4	520	2,397,072	Y
MP.5	490	1,968,952	Y
MP.6	460	5,462,365	Y
MP.10	430	5,398,139	Y
MP.9	400	—	Run-out
MP.11	430	—	Run-out
MP.13	460	4,550,671	Y
MP.15	820	29,369	Y

The results of the fatigue tests were processed, to obtain the S-N curves in the finite life domain [42]. Curves trends, together with their upper (90% failure probability) and lower (10% failure probability) bounds at the 90% confidence level, are shown in Figures 5 and 6 (with reference to Sets N, H, M, MP), using double logarithmic scale, including also details regarding specimen type, load ratio and testing frequency, as well as arrows indicating run outs. The related equations are provided in Table 8, in the terms of the coefficients of the formulas in Equations (1) and (2), considering the linear model that proved to be the most suitable, based on [42].

$$Log(N) = b_0 + b_1 \cdot Log(\sigma_i) = b_0 + b_1 \cdot S_i \quad (1)$$

$$\sigma_i = 10^{-b_0/b_1} \cdot N^{1/b_1} \quad (2)$$

Table 8. Coefficients of the determined S-N curves, according to the linear model of [42] with reference to Equations (1) and (2).

Set ID	b_0	b_1	$10^{-\frac{b_0}{b_1}}$	$\frac{1}{b_1}$
N	38.99	−12.18	1592	−0.082
H	47.73	−15.49	1207	−0.065
M	30.20	−9.06	2146	−0.110
MP	28.69	−8.26	2970	−0.121

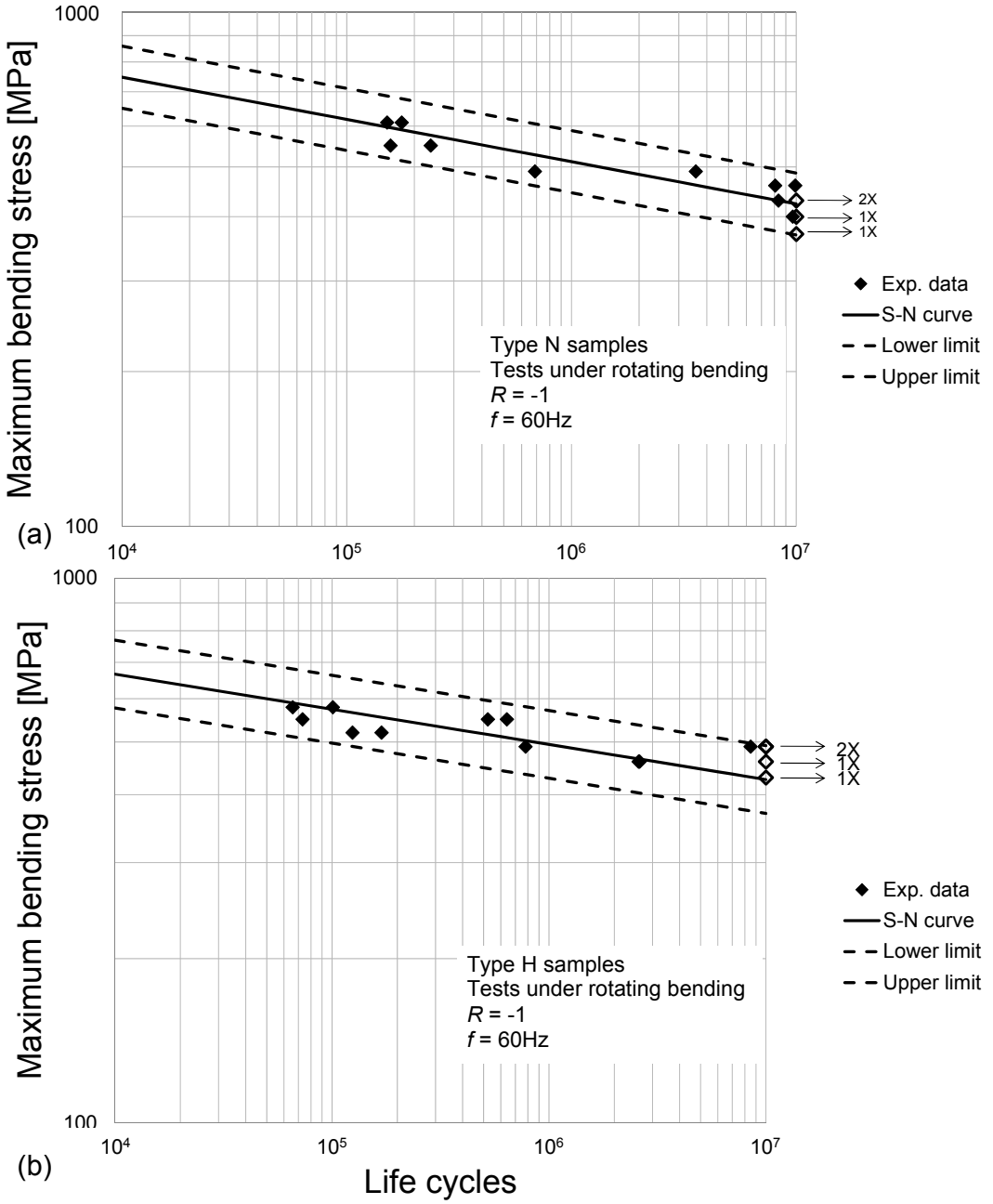

Figure 5. S-N curves along with their confidence bands with regard to Sets (**a**) N and (**b**).

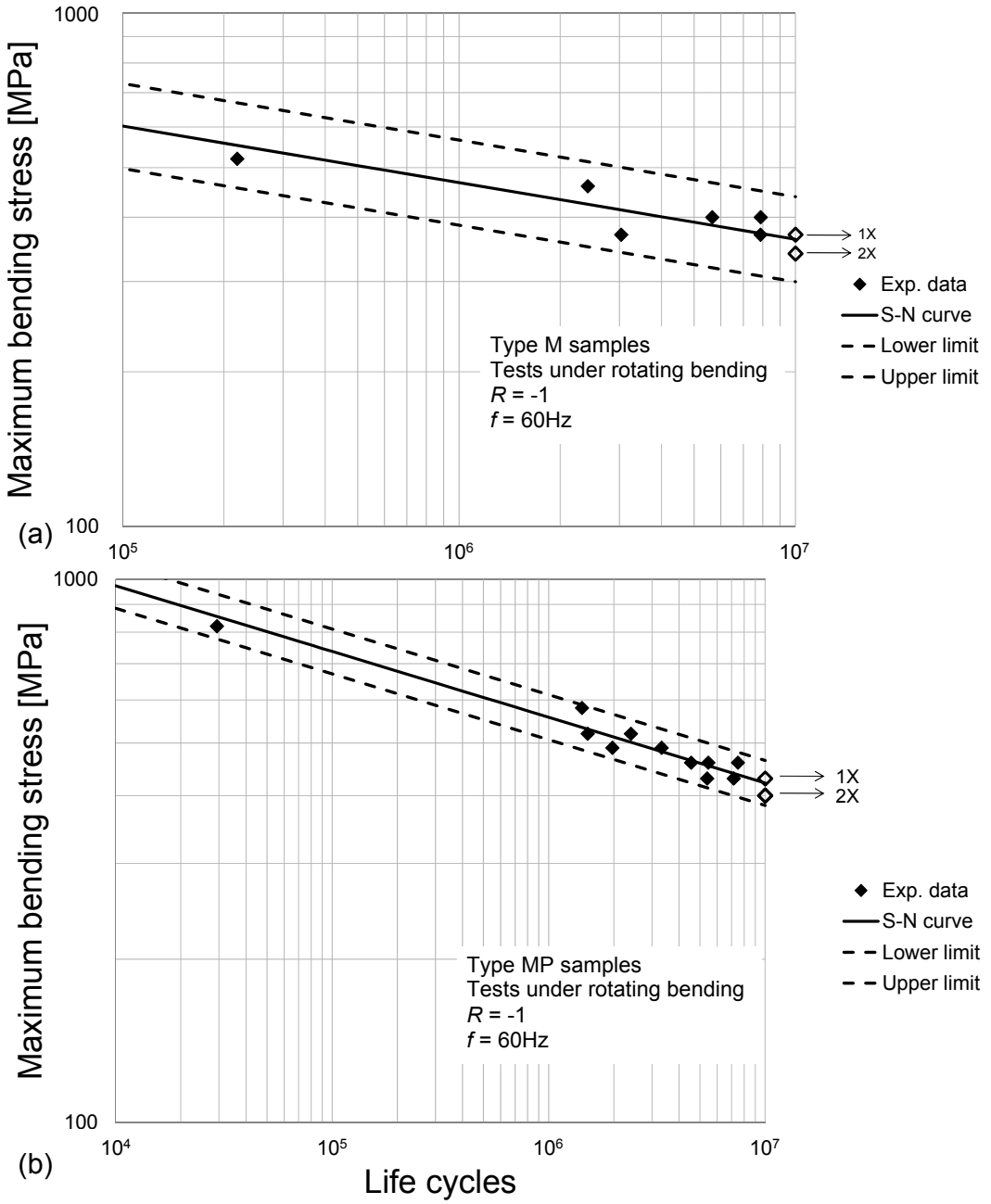

Figure 6. S-N curves along with their confidence bands with regard to Sets (**a**) M and (**b**) MP.

4. Discussion

The S-N curves in the finite life domain were processed by the ANOVA-based methodology that was introduced in [43] and successfully applied in [23], based also on more conventional applications in [44,45]. For the sake of clarity, the data-processing procedure is briefly resumed below. The first analysis involved the four treatments of the aforementioned 2-by-2 design, i.e., Sets N, M, H, and HM. In the experimental plan in Table 2, these treatments are accommodated in the first two rows and in the first two columns of the experimental design.

All the data have been processed in the logarithmic scale: in particular, S_i indicates the 10-base logarithm of σ_i, considering the fatigue curves in Table 8 and in [21,22]. As a first step, row ($\overline{S_{1.}}$, $\overline{S_{2.}}$) and column ($\overline{S_{.1}}$, $\overline{S_{.2}}$) means have been computed, combining the functions in Equations (3) to (6). In particular, $\overline{S_{1.}}$ can be regarded as the first row mean, i.e., as the mean S-N curve for the H and M

Sets being accommodated in the first row of the experimental design (Table 2). On the other hand, $\overline{S_{.1}}$ indicates the first column mean, i.e., the mean S-N curve for the treatments (Sets N and H) in the first column of the design. Similar meanings also apply to the second row mean, $\overline{S_{2.}}$, and the second column mean, $\overline{S_{.2}}$. For the sake of clarity, the conventional nomenclature for ANOVA [46] is utilized here, to indicate the mean terms and the other parameters to be determined in the following.

$$\overline{S_{1.}} = \frac{S_N + S_M}{2} \tag{3}$$

$$\overline{S_{2.}} = \frac{S_H + S_{HM}}{2} \tag{4}$$

$$\overline{S_{.1}} = \frac{S_N + S_H}{2} \tag{5}$$

$$\overline{S_{.2}} = \frac{S_M + S_{HM}}{2} \tag{6}$$

The overall mean (grand mean over all the four Sets) was then computed as reported in Equation (7):

$$\overline{S_{..}} = \frac{S_N + S_H + S_M + S_{HM}}{4} \tag{7}$$

The "Sum of Squares between Rows" (*SSBR*), i.e., the term depending on the effect of the "Row" factor, namely heat treatment, was determined as in Equation (8), where the sum of squares are weighted by the factor 2, considering that the row means are averaged over two S-N curves.

$$SSBR = \left[\left(\overline{S_{1.}} - \overline{S_{..}} \right)^2 + \left(\overline{S_{2.}} - \overline{S_{..}} \right)^2 \right] \cdot 2 \tag{8}$$

The "Sum of Squares between Columns", *SSBC*, which is related to the effect of the "Column" factor, i.e., of machining, was similarly determined as in Equation (9), where the weight factor is 2, as an effect of the column means being averaged over two fatigue curves.

$$SSBC = \left[\left(\overline{S_{.1}} - \overline{S_{..}} \right)^2 + \left(\overline{S_{.2}} - \overline{S_{..}} \right)^2 \right] \cdot 2 \tag{9}$$

Finally, the interaction term, *SSI*, was determined as in Equation (10).

$$\begin{aligned} SSI = &\left(S_N - \overline{S_{1.}} - \overline{S_{.1}} + \overline{S_{..}} \right)^2 + \left(S_H - \overline{S_{2.}} - \overline{S_{.1}} + \overline{S_{..}} \right)^2 \\ &+ \left(S_M - \overline{S_{1.}} - \overline{S_{.2}} + \overline{S_{..}} \right)^2 + \left(S_{HM} - \overline{S_{2.}} - \overline{S_{.2}} + \overline{S_{..}} \right)^2 \end{aligned} \tag{10}$$

Regarding *SSBR*, *SSBC*, and *SSI*, the related functions were converted into scalars by the computation of their integral means over the lifespan considered in the fatigue campaign in the finite life domain. The error term was finally determined as the sum of the squares of the residuals between the actual experimental data and the predicted ones based on the S-N curves.

All the data were then processed as a conventional two-way *ANOVA*, provided that the sum of squares terms were scaled, dividing them by the related degrees of freedom. The Analysis of Variance was followed by the Fisher test, to discuss the significance of the effects of the heat treatment and of machining along with their interaction. The outcome (reported in Table 9), based on a lifespan ranging from 10^4 to 10^7, was that both factors were highly significant, accepting a probability of error, commonly regarded as p-value, in the order of 10^{-5}. The interaction is also significant with a p-value around 10^{-6}.

Table 9. ANOVA Table for the two-factor design (lifespan between 10^4 and 10^7).

	Sum of Squares	Degrees of Freedom	Failure	Fisher's Ratio	*p*-Value
SSBR: Effect of the heat treatment	0.0164	1	0.0164	19.71	3×10^{-5}
SSBC: Effect of machining	0.0187	1	0.0187	22.51	10^{-5}
SSI: Interaction	0.0236	1	0.0236	28.39	10^{-6}
SSE: Error	0.0633	76	0.0008		

The four curves, corresponding to the sets referenced as N, M, H, and HM are plotted together in the graph in Figure 7. It can be observed that, starting from the curve for Set N, colored in black, the red one for Set H is very close, whereas the yellow one for Set M indicates a slightly lower strength.

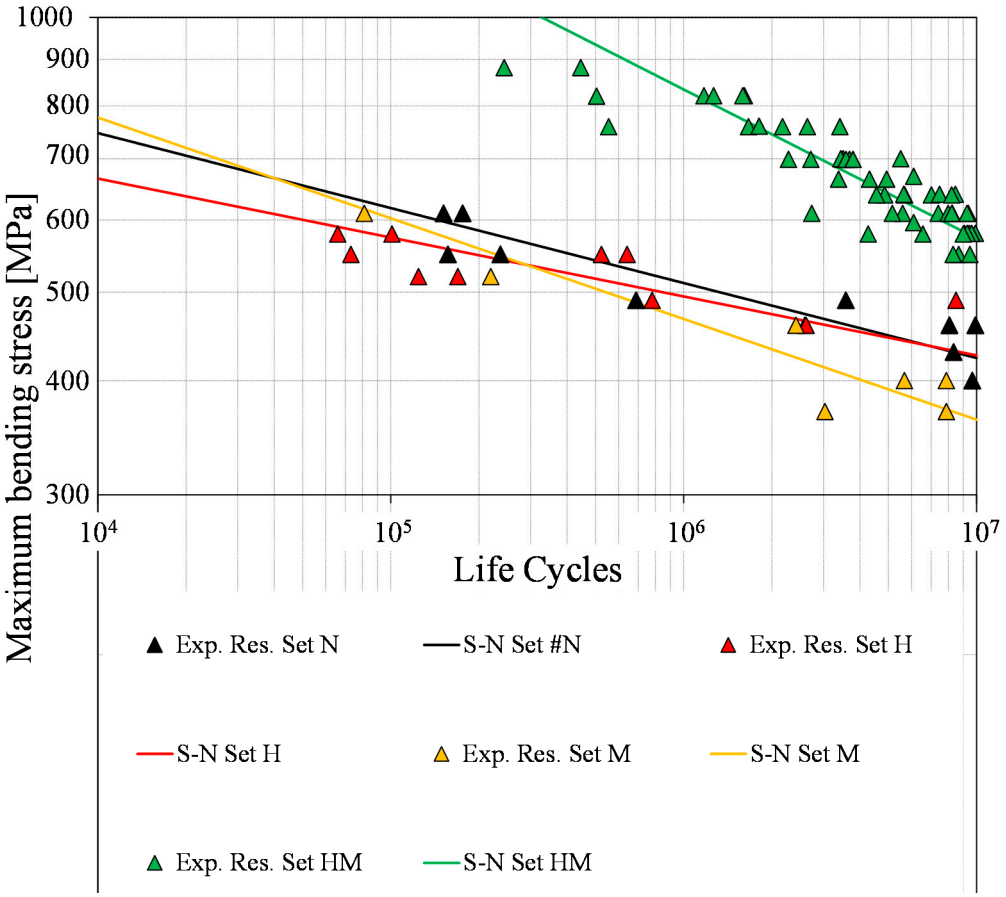

Figure 7. Comparison between the S-N curves in the finite life domain for Sets N, M, H, and HM.

These results were interpreted in the light of a further analysis. The same procedure being described in [43], regarding one-way ANOVA, was here applied to compare the two curves (black and red) corresponding to the Sets (N and H) in the as-built state with and without heat treatment. The same procedure was subsequently applied to compare the S-N plots (black and yellow) for the samples without heat treatment in the as-fabricated state (Set N) or that underwent machining (Set M). In both cases, the statistical tests indicate the differences between the couples of curves are not significant. In other words, the curve for Set N is statistically the same as that for Set H and also as that for Set M. Regarding the effect of heat treatment without machining, it must be remarked that the build process of a Maraging Steel usually leads to a not-high-tensile residual stress field, due to the low coefficient of thermal expansion (CTE), if compared to that of other materials, e.g., Stainless Steel 15-5 PH [23].

In fact, the lower the CTE, the lower the induced residual stresses [23,47]. Therefore, considering the lower amount of residual stresses, being also reduced by micro-shot-peening, the application of heat treatment becomes ineffective. In other words, the peening treatment seems to provide a sufficient contribution against the process-induced not remarkably high tensile residual stresses.

The further outcome of the performed analysis, i.e., the counter-intuitive slightly detrimental effect of machining, especially regarding the fatigue limit, can be explained with reference to the beneficial compressive residual stresses induced by micro-shot-peening being removed by machining. This result indicates that the positive effect of surface finishing is compensated by the simultaneous removal of the superficial layers, where the peening-induced compressive state was able to provide some protection against crack propagation. This effect can be observed in the not-heat-treated samples, where micro-shot-peening plays indeed an important role at relaxing the detrimental tensile residual stresses, as also remarked in the previous paragraph.

Finally, regarding the forth curve, the green one for the HM condition, it keeps much higher than all the others. It indicates the high positive interaction between the two considered factors: in other words, if they are applied together, they have a synergic effect at remarkably enhancing the fatigue strength. On one hand, the heat treatment becomes highly beneficial on a refined surface, when the effect of shot peening is removed through machining. On the other hand, machining is also significantly beneficial, as it refines the surface, while simultaneously the heat treatment drops down the residual stress state induced by the stacking process (while the effect of the peening treatment is completely removed).

It is important to make a specific remark about the effect of the aging heat treatment. This seems to be highly effective, only if it is carried out on a refined surface, whereas its effect drops down to zero, and may be even detrimental, when it is performed on a coarse surface in the as-built state. A possible reason for this occurrence is that the aging treatment makes the Maraging steel much more notch-sensitive. This property is commonly related to the increase of the material UTS, which is actually remarkably incremented by the aging treatment according to ref. [14,38]. Therefore, the aging treatment turns to be highly beneficial only on a machined refined surface, but may be detrimental on as-built parts with surface asperities and process-induced defects at a sub-surface level. Regarding this point, some results by fractographic analyses are provided in the following.

A final analysis was conducted, also including the curve for the MP Set. The S-N curves for Sets N, M, and MP, i.e., for all the Sets, which did not undergo the aging treatment, are plotted together in Figure 8. The tool of one-way ANOVA with three levels has been utilized to compare the three curves, as concisely described below.

A grand mean curve $\overline{S_{..}}'$ has initially been computed as in Equation (11), where S indicates the 10-base logarithm of the stress corresponding to a generic fatigue life, and the subscript refers to the Set type, according to Tables 2 and 8. $\overline{S_{..}}'$ can be regarded as the grand mean of the S-N curves of all the sets with different treatments in the first row of Table 2. The ANOVA nomenclature [46] is again used to indicate the mean and the sum of squares.

$$\overline{S_{..}}' = \frac{S_N + S_M + S_{MP}}{3} \tag{11}$$

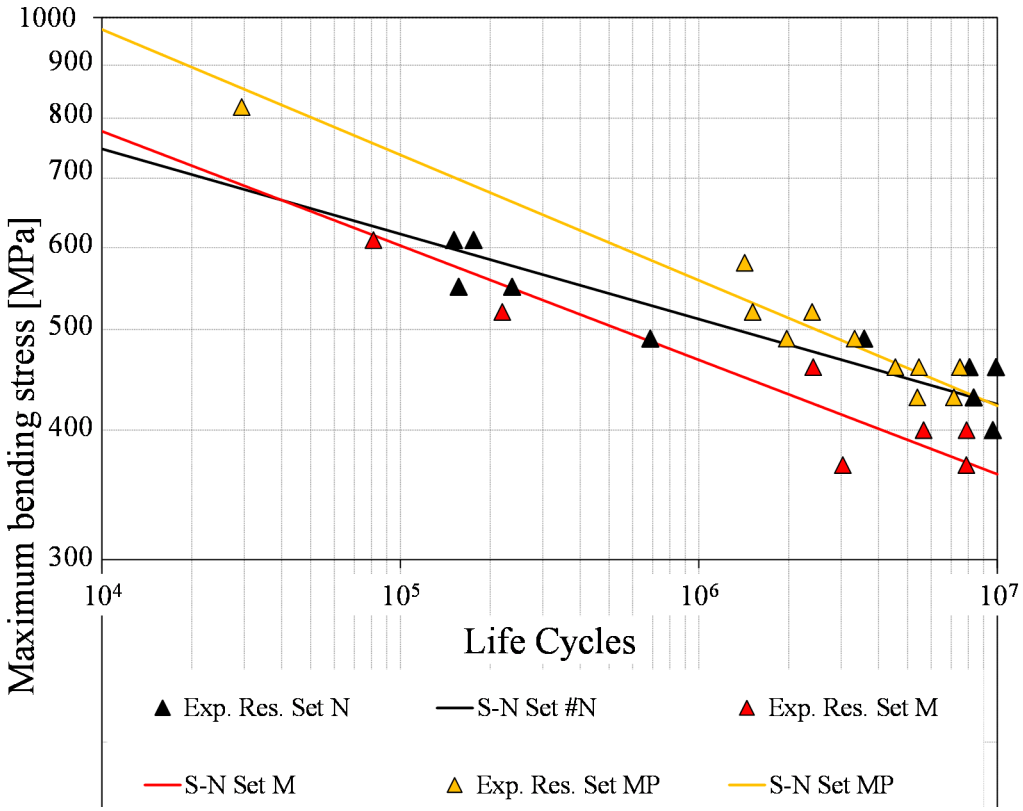

Figure 8. Comparison between the S-N curves in the finite life domain for Sets N, M, and MP.

Then, an "*SSBC′*" term, being related to the effect of post-processing (machining, shot-peening, and related order), has been determined as in Equation (12).

$$SSBC' = \left(S_N - \overline{S_{..}}'\right)^2 + \left(S_M - \overline{S_{..}}'\right)^2 + \left(S_{MP} - \overline{S_{..}}'\right)^2 \quad (12)$$

As above, the error term was estimated as the sum of the squares of the residuals between the experimental actual yields and the estimated ones, according to the determined fatigue curves. Scalar terms were then worked out as the integral means of the quadratic terms over the investigated life span. The analysis proceeded as a conventional one-factor ANOVA after scaling the scalar terms that were divided by their degrees of freedom.

The result was that the fatigue strength in the finite life domain is significantly incremented, when shot-peening is performed after machining, i.e, when the curve for the MP Set is compared to the other two. This outcome is a further proof for the importance of shot-peening: applying it after machining makes it possible to take advantage of both the induced compressive residual stress (which compensates for that induced by the building process, in absence of heat treatment) and the better surface finishing.

The fatigue limits for all the sample types with their confidence band (90% confidence level) are shown in the bar graph in Figure 9. As mentioned above, the fatigue limits were worked out by the Dixon method with related confidence analysis, except for Set HM: in this case, the fatigue limit was extrapolated by the S-N curve as the stress corresponding to an expected life of 10^7 cycles. The scatter evaluated in the finite life region was also applied at the fatigue limit, while keeping the same level of confidence for comparison purposes [48]. The estimated value of FL for sample type HM is 573 MPa, for sample type H is 471 MPa, for sample type N is 426 MPa, for sample type M is 363 MPa, and for Set MP is 423 MPa. The sample sets named H and HM underwent heat treatment, whereas the other threes did not undergo heat treatment. The UTS of MS1 Maraging Steel is 1100 MPa in the as-built

condition; after hardening, it is drastically incremented up to 2050 MPa, corresponding to almost 100% increase of UTS following heat treatment [38].

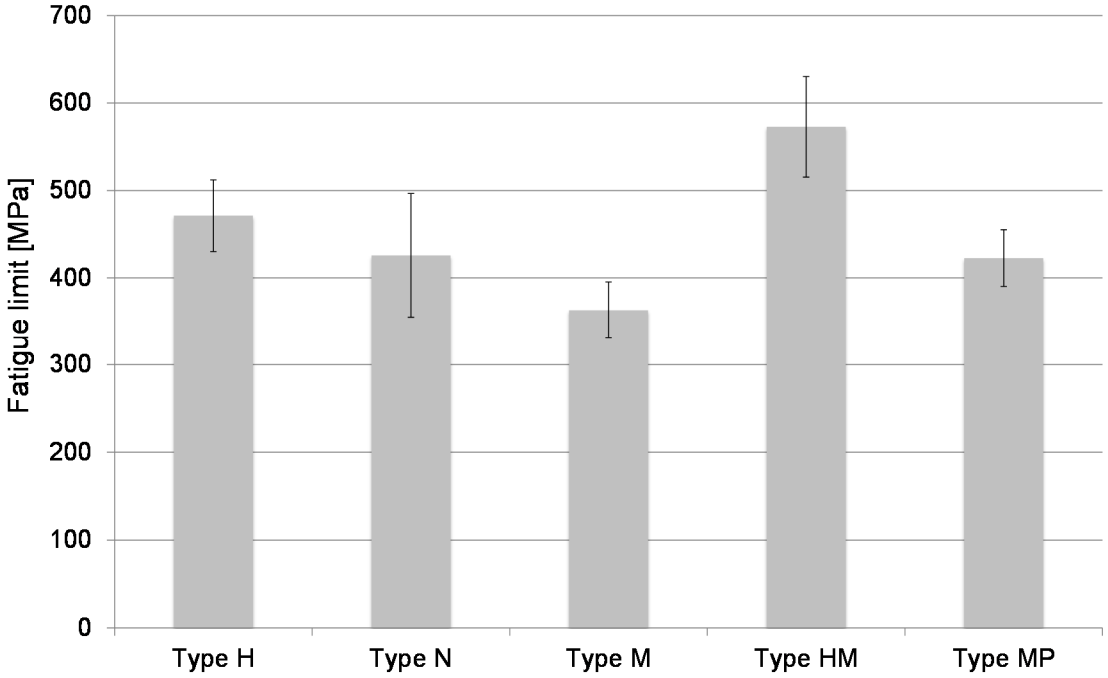

Figure 9. Fatigue limits for 10 million cycle run-out with regard to all the sample Sets in the experimental design.

Regarding Sample types HM and H, their FL is respectively 28% and 23% of UTS. Sample types N, M, and MP were without hardening and their FL is, as expected, indeed lower, but respectively, 38%, 33%, 38% of the corresponding UTS for the not heat-treated material. Moreover, the Sets N and MP have very close FLs, whereas the latter yields much better performance for finite life, as remarked above. This indicates that the effect of shot-peening after machining turns out to be negligible for infinite life. These ratios are much lower than the commonly accepted ratios of FL over UTS of 50% for wrought material following machining, but are in agreement with some literature research, when considering as-built parts [49,50]. This is not surprising, due to the layered characteristic of specimens. Sample type N proved to have a greater FL than machined sample type M.

During fractographic and micrographic analysis, some porosities were observed. During the fractographic analysis of both the surfaces of the broken sample, it was found that crack initiation usually occurs at one point on the surface or, more frequently, just beneath it, at a distance of about 80 μm from the edge. Some amount of voids and inclusions were noticed on fractured surfaces of all samples. It is indeed possible that voids or inclusions were responsible for crack initiation: most cracks seem to actually start from these defects. Only one crack initiation point was generally observed. Some examples of fractures that initiated from sub-surface defects are depicted in Figure 10 with regard to all the Sets involved in the experimental campaign.

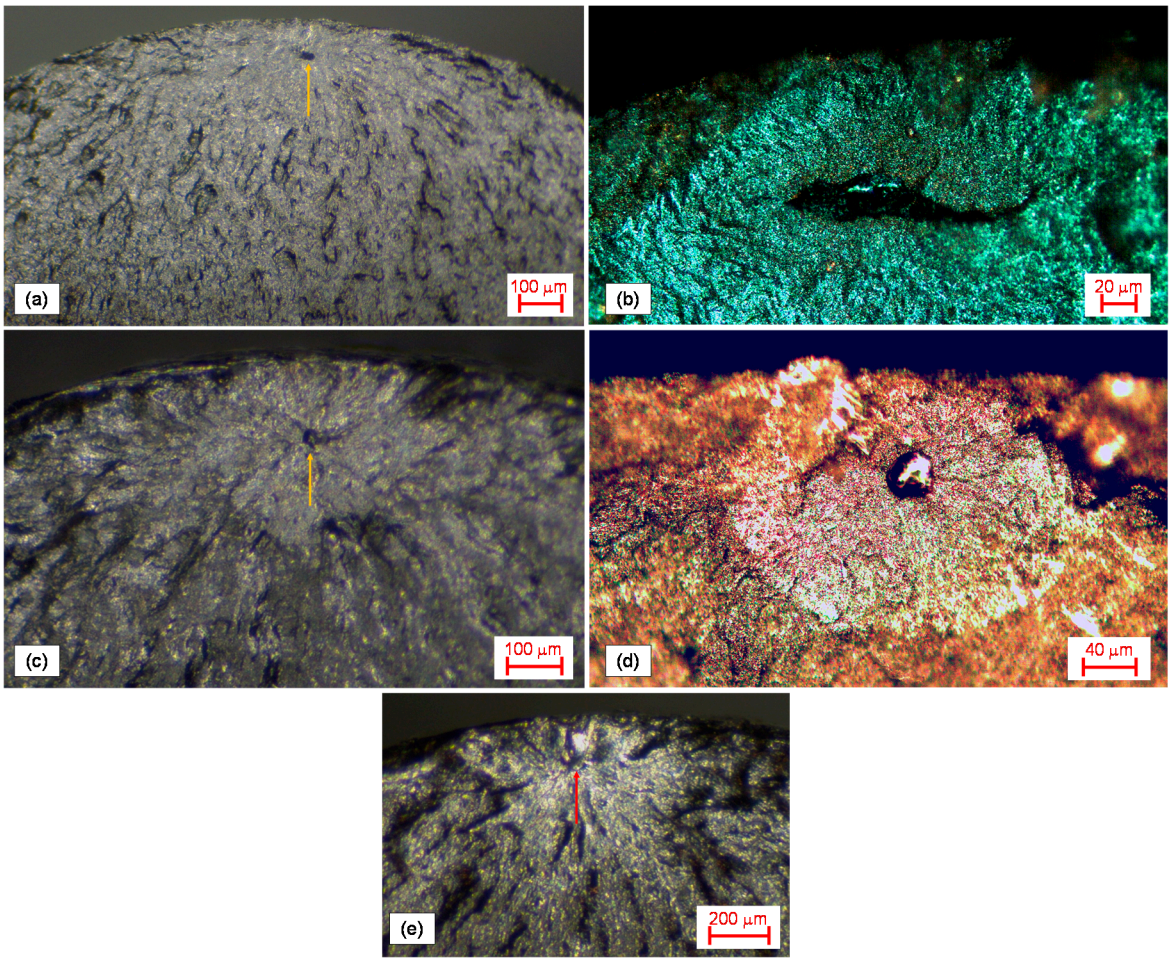

Figure 10. (**a**) A crack initiating from a porosity in a sample of Set M (by stereo-microscope); (**b**) a large void that triggered a failure in a specimen of Set H (by optical microscope); cracks initiating from sub-surface porosities in samples of Sets (**c**) N (by stereo-microscope); (**d**) HM (by optical microscope) and (**e**) MP (by stereo-microscope).

Micrographies indicated that laser scanning traces were visible both in longitudinal and in transverse sections, regardless of heat treatment execution. Some inclusions were noticed and are marked with circles in Figure 11, which refers to a sample of Set N. The scanning pattern in the build plane section in Figure 11a indicates some scanning traces underneath with rotation angles corresponding to the aforementioned angle of 67°. Specimens without heat treatment, like those Figure 11 refers to, had more pronounced scanning traces than those that had undergone the heat treatment by age hardening, which had, conversely, a more uniform microstructure. The microstructure of a sample of Set H is shown in Figure 12. This outcome indicates that heat treatment had some effect on fusion of the laser traces but was not effective at completing deleting these traces. For all the sample types, a comparable amount of inclusion was observed. Heat treatment had no effect on the presence of porosities in material.

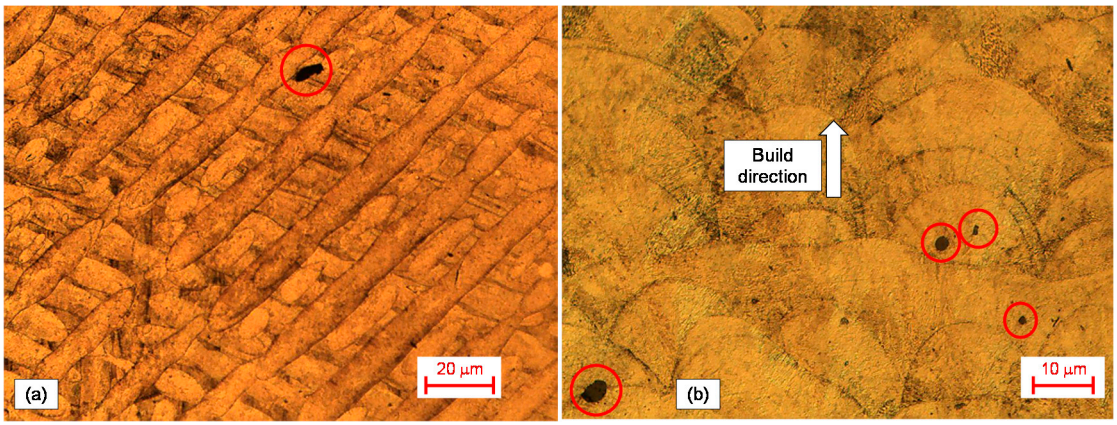

Figure 11. Micrographies on a sample of Set N (without heat treatment) depicting (**a**) laser scans over the build plane and (**b**) stacked layers along the build direction. Inclusions are also highlighted.

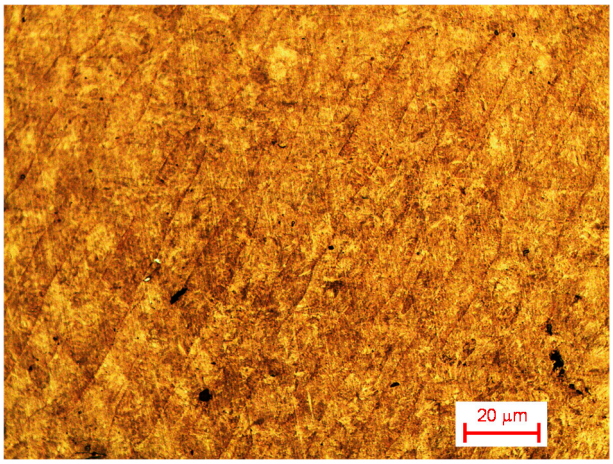

Figure 12. Micrography on a sample of Set H (with heat treatment), depicting laser scans over the build plane (cross section).

5. Conclusions

This paper has dealt with a study on machining and heat and surface treatment effects on fatigue limit and fatigue strength of Maraging Steel specimens manufactured by DMLS EOSINT M280 machine. Five sample sets were considered, all with vertical stacking direction during building. All four initial sets underwent micro-shot-peening after the building process. One Set was tested in the as-built condition, without heat treatment; a second one underwent an aging heat treatment but was kept in the as-fabricated state. A third set was machined without heat treatment. Finally, an S-N curve coming from previous studies was used for comparison: it refers to samples that underwent heat treatment and then machining, as recommended by the material manufacturer. All the experimental results were processed for the determination of S-N curves in the finite life domain and fatigue limits. Statistical methods were used to compare the curves, and their outcomes indicated that heat treatment without machining has a negligible effect, as micro-shot-peening is able to reduce the process-induced residual stress state, which is not particularly high due to material properties. The generally positive effect of machining is compensated by the removal of the surface layers treated by micro-shot-peening, when heat treatment is not performed. Finally, when heat treatment and machining are applied together, they have a synergic beneficial effect, and the fatigue strength is remarkably incremented. A possible reason for the observed occurrences is that the aging treatment makes the Maraging steel much more notch-sensitive. Therefore, this treatment is highly beneficial on refined surfaces, but may even be

detrimental on unmachined parts with high roughness at the surface and process-induced porosities just beneath it.

A fifth set was added to the experiment to investigate if performing the peening treatment after machining without heat treatment could have a positive effect on the fatigue strength. The statistical analysis confirmed this outcome: refining the surface and then applying a compressive residual stress state leads to a fatigue enhancement in the finite life domain. It is important to remark that a good tuning of the post-process parameters can lead to a fatigue limit in the order of almost 40% of the ultimate tensile strength, just ten points lower than the commonly accepted 50% ratio for wrought material.

The study was completed by fractographic and micrographic analyses. The first ones made it possible to individuate some porosities, which were the main sources for crack initiation at approximately 80 µm from the surface. The second one made it possible to compare the microstructures with and without the heat treatment. In the first case, the scanning traces are still visible, but the microstructure is made more uniform.

As a future development of this research, the case of shot-peening being performed on heat-treated and machined samples will be considered. Moreover, it will be also the chance to investigate the effect of the position in the chamber on the fatigue response.

Author Contributions: Methodology, D.C., G.O. and A.V.; Sample fabrication and post-processing, S.Ć.K., A.V. and N.B.; Fatigue testing, M.D.A, S.F., G.O, F.R. and A.V.; Data statistical processing, G.O. and D.C.; Fractography and Micrography, M.D.A., S.F., G.O. and A.V.; Original Draft Paper writing, G.O. and A.V.; Revised Paper writing, G.O.; Supervision, D.C. and G.O.; Funding Acquisition, S.Ć.K. and D.C.

Funding: The research presented in this paper has received funding from the European Union's Horizon 2020 research and innovation programme under the Marie Skłodowska-Curie grant agreement No. 734455.

Conflicts of Interest: The authors declare no conflict of interest.

References

1. Bourell, D.L.; Beaman, J.J.; Leu, M.C.; Rosen, D.W. A brief history of additive manufacturing and the 2009 roadmap for additive manufacturing: Looking back and looking ahead. In Proceedings of the RapidTech, Istanbul, Turkey, 24–25 September 2009.
2. Aliakbari, M. Additive Manufacturing: State-Of-The-Art, Capabilities, and Sample Applications with Cost Analysis. Master's Thesis, Production Engineering and Management, Department of Industrial Production, KTH, Stockholm, Sweden, 2012.
3. Pandey, P.M. *Rapid Prototyping Technologies, Applications and Part Deposition Planning*; Department of Mechanical Engineering, Indian Institute of Technology: Delhi, India, 2010.
4. Herderick, E. Additive Manufacturing of Metals: A Review. In Proceedings of the Materials Science and Technology (MS&T), Columbus, OH, USA, 16–20 October 2011; pp. 1413–1425.
5. Shellabear, M.; Nyrhilä, O. DMLS-Development history and state of the art. In Proceedings of the 4th Laser Assisted Netshape Engineering (LANE), Erlangen, Germany, 21–24 September 2004.
6. Nicoletto, G. Directional and notch effects on the fatigue behavior of as-built DMLS Ti6Al4V. *Int. J. Fatigue* **2018**, *106*, 124–131. [CrossRef]
7. International Organization for Standardization. *Additive Manufacturing—General Principles—Terminology*; ISO/ASTM 52900:2015 (ASTM F2792); International Organization for Standardization (ISO): Geneva, Switzerland, 2015.
8. Campanelli, S.L.; Contuzzi, N.; Angelastro, A.; Ludovico, A.D. Capabilities and performances of the selective laser melting process. In *New Trends in Technologies: Devices, Computer, Communication and Industrial Systems (InTech)*; Intech Open Limited: London, UK, 2010.
9. Naiju, C.D.; Adithan, M.; Radhakrishnan, P. An Investigation of Process Variables Influencing Fatigue Properties of Components Produced by Direct Metal Laser Sintering. *KMUTNB IJAST* **2011**, *4*, 63–69.
10. Parthasarathy, J.; Starly, B.; Raman, S. A design for the additive manufacture of functionally graded porous structures with tailored mechanical properties for biomedical applications. *J. Manuf. Process.* **2011**, *13*, 160–170. [CrossRef]

11. Jardini, A.L.; Larosa, M.A.; Macedo, M.F.; Bernardes, L.F.; Lambert, C.S.; Zavaglia, C.A.C.; Maciel Filho, R.; Calderoni, D.R.; Ghizoni, E.; Kharmandayan, P. Improvement in Cranioplasty: Advanced Prosthesis Biomanufacturing. *Proc. CIRP* **2016**, *49*, 203–208. [CrossRef]
12. Jardini, A.L.; Larosa, M.A.; Maciel Filho, R.; de Carvalho Zavaglia, C.A.; Bernardes, L.F.; Lambert, C.S.; Calderoni, D.R.; Kharmandayan, P. Cranial reconstruction: 3D biomodel and custom-built implant created using additive manufacturing. *J. Cranio Maxillofac. Surg.* **2014**, *42*, 1877–1884. [CrossRef] [PubMed]
13. Bertol, L.S.; Júnior, W.K.; da Silva, F.P.; Aumund-Kopp, C. Medical design: Direct metal laser sintering of Ti–6Al–4V. *Mater. Des.* **2010**, *31*, 3982–3988. [CrossRef]
14. EOS GmbH. Available online: https://www.eos.info/material-m (accessed on 28 June 2018).
15. Brookes, K.J. Maraging steel for additive manufacturing—Philipp Stoll's paper at DDMC 2016. *Met. Powder Rep.* **2016**, *71*, 149–152. [CrossRef]
16. Yasa, E.; Kempen, K.; Kruth, J.P.; Thijs, L.; Van Humbeeck, J. Microstructure and mechanical properties of maraging steel 300 after selective laser melting. In Proceedings of the 21st International Solid Freeform Fabrication Symposium, Austin, TX, USA, 9–11 August 2010; pp. 383–396.
17. Kempen, K.; Yasa, E.; Thijs, L.; Kruth, J.P.; Van Humbeeck, J. Microstructure and mechanical properties of Selective Laser Melted 18Ni-300 steel. *Phys. Procedia* **2011**, *12*, 255–263. [CrossRef]
18. Casalino, G.; Campanelli, S.L.; Contuzzi, N.; Ludovico, A.D. Experimental investigation and statistical optimisation of the selective laser melting process of a maraging steel. *Opt. Laser Technol.* **2015**, *65*, 151–158. [CrossRef]
19. EOS GmbH. Available online: https://www.eos.info/press/customer_case_studies/gripper (accessed on 28 June 2018).
20. Branco, R.; Costa, J.D.M.; Berto, F.; Razavi, S.M.J.; Ferreira, J.A.M.; Capela, C.; Santos, L.; Antunes, F. Low-Cycle Fatigue Behaviour of AISI 18Ni300 Maraging Steel Produced by Selective Laser Melting. *Metals* **2018**, *8*, 32. [CrossRef]
21. Croccolo, D.; De Agostinis, M.; Fini, S.; Olmi, G.; Vranic, A.; Ciric-Kostic, S. Influence of the build orientation on the fatigue strength of EOS maraging steel produced by additive metal machine. *Fatigue Fract. Eng. Mater. Struct.* **2016**, *39*, 637–647. [CrossRef]
22. Croccolo, D.; De Agostinis, M.; Fini, S.; Olmi, G.; Robusto, F.; Muharemovic, N.; Bogojevic, N.; Vranic, A.; Ciric-Kostic, S. Experimental study on the sensitivity of DMLS manufactured Maraging Steel fatigue strength to the build orientation and allowance for machining. In Proceedings of the 6th International Conference Integrity-Reliability-Failure (IRF 2018), Lisbon, Portugal, 22–26 July 2018.
23. Croccolo, D.; De Agostinis, M.; Fini, S.; Olmi, G.; Bogojevic, N.; Ciric-Kostic, S. Effects of build orientation and thickness of allowance on the fatigue behaviour of 15–5 PH stainless steel manufactured by DMLS. *Fatigue Fract. Eng. Mater. Struct.* **2018**, *41*, 900–916. [CrossRef]
24. Casati, R.; Lemke, J.N.; Tuissi, A.; Vedani, M. Aging Behaviour and Mechanical Performance of 18-Ni 300 Steel Processed by Selective Laser Melting. *Metals* **2016**, *6*, 218. [CrossRef]
25. Gibson, I.; Shi, D. Material properties and fabrication parameters in selective laser sintering process. *Rapid Prototyp. J.* **1997**, *3*, 129–136. [CrossRef]
26. Baufeld, B.; Van der Biest, O.; Gault, R. Additive manufacturing of Ti–6Al–4V components by shaped metal deposition: Microstructure and mechanical properties. *Mater. Des.* **2010**, *31* (Suppl. 1), S106–S111. [CrossRef]
27. Edwards, P.; Ramulu, M. Fatigue performance evaluation of selective laser melted Ti–6Al–4V. *Mater. Sci. Eng. A* **2014**, *598*, 327–337. [CrossRef]
28. Bača, A.; Konečná, R.; Nicoletto, G.; Kunz, L. Influence of build direction on the fatigue behaviour of Ti6Al4V alloy produced by direct metal laser sintering. *Mater. Today* **2016**, *3*, 921–924. [CrossRef]
29. Konečná, R.; Kunz, L.; Bača, A.; Nicoletto, G. Long fatigue crack growth in Ti6Al4V produced by direct metal laser sintering. *Proc. Eng.* **2016**, *160*, 69–76. [CrossRef]
30. Smith, D.H.; Bicknell, J.; Jorgensen, L.; Patterson, B.M.; Cordes, N.L.; Tsukrov, I.; Knezevic, M. Microstructure and mechanical behavior of direct metal laser sintered Inconel alloy 718. *Mater. Charact.* **2016**, *113*, 1–9. [CrossRef]
31. Brandl, E.; Heckenberger, U.; Holzinger, V.; Buchbinder, D. Additive manufactured AlSi10Mg samples using Selective Laser Melting (SLM): Microstructure, high cycle fatigue, and fracture behavior. *Mater. Des.* **2012**, *34*, 159–169. [CrossRef]

32. Lewandowski, J.J.; Seifi, M. Metal Additive Manufacturing: A Review of Mechanical Properties. *Annu. Rev. Mater. Res.* **2016**, *46*, 151–186. [CrossRef]
33. Yadollahi, A.; Shamsaei, N.; Thompson, S.M.; Elwany, A.; Bian, L. Effects of building orientation and heat treatment on fatigue behavior of selective laser melted 17-4 PH stainless steel. *Int. J. Fatigue* **2017**, *94*, 218–235. [CrossRef]
34. Agius, D.; Kourousis, K.I.; Wallbrink, C. A Review of the As-Built SLM Ti-6Al-4V Mechanical Properties towards Achieving Fatigue Resistant Designs. *Metals* **2018**, *8*, 75. [CrossRef]
35. Blinn, B.; Klein, M.; Gläßner, C.; Smaga, M.; Aurich, J.C.; Beck, T. An Investigation of the Microstructure and Fatigue Behavior of Additively Manufactured AISI 316L Stainless Steel with Regard to the Influence of Heat Treatment. *Metals* **2018**, *8*, 220. [CrossRef]
36. International Organization for Standardization. *Metallic Materials—Rotating Bar Bending Fatigue Testing*; ISO 1143:2010 (E) (2010); International Organization for Standardization (ISO): Geneva, Switzerland, 2010.
37. EOS GmbH. Available online: https://www.eos.info/systems_solutions/metal/systems_equipment/eosint_m280 (accessed on 28 June 2018).
38. EOS GmbH. Available online: https://www.eos.info/material_m/werkstoffe/download/EOS_MaragingSteel_MS1.pdf (accessed on 28 June 2018).
39. Sanz, C.; Navas, V.G. Structural integrity of direct metal laser sintered parts subjected to thermal and finishing treatments. *J. Mater. Process. Technol.* **2013**, *213*, 2126–2136. [CrossRef]
40. Aboulkhair, N.T.; Maskery, I.; Tuck, C.; Ashcroft, I.; Everitt, N.M. Improving the fatigue behaviour of a selectively laser melted aluminium alloy: Influence of heat treatment and surface quality. *Mater. Des.* **2016**, *104*, 174–182. [CrossRef]
41. Dixon, W.J.; Massey, F.J. *Introduction to Statistical Analysis*; McGraw-Hill: New York, NY, USA, 1969.
42. International Organization for Standardization. *Metallic Materials—Fatigue Testing—Statistical Planning and Analysis of Data*; ISO 12107:2012; International Organization for Standardization (ISO): Geneva, Switzerland, 2012.
43. Olmi, G. Low cycle fatigue experiments on Turbogenerator steels and a new method for defining confidence bands. *J. Test. Eval.* **2012**, *40*, 1–14. [CrossRef]
44. Croccolo, D.; De Agostinis, M.; Fini, S.; Olmi, G. Influence of the engagement ratio on the shear strength of an epoxy adhesive by push-out tests on pin-and-collar joints: Part I: Campaign at room temperature. *Int. J. Adhes. Adhes.* **2016**, *67*, 69–75. [CrossRef]
45. Croccolo, D.; De Agostinis, M.; Fini, S.; Olmi, G. Influence of the engagement ratio on the shear strength of an epoxy adhesive by push-out tests on pin-and-collar joints: Part II: Campaign at different temperature levels. *Int. J. Adhes. Adhes.* **2016**, *67*, 76–85. [CrossRef]
46. Berger, P.D.; Maurer, R.E. *Experimental Design with Applications in Management, Engineering and the Sciences*; Duxbury Press: Belmont, CA, USA, 2002.
47. Fergani, O.; Berto, F.; Welo, T.; Liang, S.Y. Analytical modelling of residual stress in additive manufacturing. *Fatigue Fract. Eng. Mater. Struct.* **2017**, *40*, 971–978. [CrossRef]
48. Meneghetti, G.; Dengo, C.; Lo Conte, F. Bending fatigue design of case-hardened gears based on test specimens. *Proc. IMechE Part C J. Mech. Eng. Sci.* **2017**. [CrossRef]
49. Stoffregen, H.A.; Butterweck, K.; Abele, E. Fatigue analysis in selective laser melting: Review and investigation of thin-walled actuator housings. In Proceedings of the 25th Solid Freeform Fabrication Symposium, Austin, TX, USA, 4–6 August 2014.
50. Niemann, G.; Winter, H.; Hohn, B.R. *Maschinenelemente*; Springer: Berlin, Germany, 2005.

© 2018 by the authors. Licensee MDPI, Basel, Switzerland. This article is an open access article distributed under the terms and conditions of the Creative Commons Attribution (CC BY) license (http://creativecommons.org/licenses/by/4.0/).